Modeling of Ductile Failure in Destructive Manufacturing Processes Using the Smoothed Particle Galerkin Method

Youcai Wu, C.T. Wu, Wei Hu

Livermore Software Technology Corporation (LSTC)
7374 Las Positas Road, Livermore, CA 94551, U.S.A.

Abstract

In this paper, ductile failure in destructive manufacturing processes such as friction drilling of metals is modeled using an authentic meshfree method, i.e., the smoothed particle Galerkin (SPG) method. To improve the efficiency and stability of the numerical scheme, the SPG weak form is integrated using the direct nodal integration (DNI) technique that is stabilized by a non-residual penalty type stabilization term derived from displacement. The SPG theory is briefly reviewed and the SPG bond failure mechanism for material failure analysis is elaborated in this paper. The setup for an LS-DYNA® SPG analysis is also presented. To demonstrate the performance of the SPG method, a metal friction drilling process is analyzed using the SPG formulation. The sensitivity of the numerical results to the SPG bond failure criteria, the nodal support size, the frequency of SPG kernel updating, and the coefficient of friction is thoroughly studied in the numerical example. The results are also compared to limited experimental data.

Keywords: failure analysis, smoothed particle Galerkin (SPG), destructive manufacturing

1. Introduction

Material failure frequently occurs in destructive manufacturing processes in aerospace industry, automotive industry, electronics industry, furniture manufacturing and other applications such as FDS (flow drill screw), SPR (self pierce riveting), metal blanking, cutting, drilling, grinding, machining, shearing, tapping, etc. To obtain the desired outcome from these processes is difficult due to many parameters such as operation speed, material properties, interface friction, geometry design, etc. It is not practical to conduct the experiments in order to obtain the optimized designs because of the cost and time. Therefore, numerical analysis has been playing an important role in the design of these manufacturing processes.

Traditionally, finite element method (FEM) is applied in all sorts of CAE (computer aided engineering) analysis, such as compression molding, extrusion, forging, spring back, etc. Large deformation occurs in these processes, but material failure is less likely to occur. To deal with material failure in destructive manufacturing processes, element erosion technique is widely applied in finite element (FE) approach. The criterion for element erosion is usually ad-hoc and the results are very sensitive to the criterion. Meanwhile, adaptive FEM and EFG (element free Galerkin) are also developed to deal with this type large deformation induced material failure. However, the process is tedious and not user friendly. Based on the element erosion technique, SPH (smoothed particle hydrodynamics) and ALE (arbitrary Lagrangian Eulerian) approaches are also

applied in the analysis of material failure. Nonetheless, SPH is known to have various numerical deficiencies such as lack of consistency, tension instability, spurious energy modes, and complication in enforcing essential boundary conditions. Both SPH and ALE have difficulty in tracking the formation of new surfaces and are not able to prevent material self-healing in failure analysis.

To more physically treat material failure in destructive manufacturing processes, a genuine meshfree method, the smoothed particle Galerkin (SPG) method [1, 2, 3], was developed recently. The SPG method is a residual based Galerkin meshfree method. Its weak form is integrated using the direct nodal integration (DNI) technique to improve computational efficiency. A strain operator derived from displacement smoothing theory is used in the SPG formulation for stabilizing the DNI scheme. This stabilization formulation is parameterized by a measure of the local length scale without using a stabilization control parameter. As such, the SPG formulation has been applied to the analysis of damage-induced strain localization in elastic materials [3], ductile fracture in two-dimensional explicit dynamics [4], three-dimensional concrete perforation and penetration [5] and three-dimensional destructive metal grinding applications [6].

In this paper, the SPG method is employed to analyze the ductile failure in a metal friction drilling process along with sensitivity study of the SPG parameters. The remaining of this paper is organized as follows: the basic SPG formulations and the strain based SPG bond failure mechanism are introduced in Section 2. Section 3 presents the application of the SPG method in the analysis of a friction drilling process. Concluding remarks are made in the final section.

2. Formulations

2.1. The SPG shape function

The strong form of a boundary – initial value problem can be stated as: find the displacement field $\mathbf{u}(\mathbf{x},t)$ such that:

$$\rho\ddot{\mathbf{u}}(\mathbf{x},t) - \boldsymbol{\sigma}(\mathbf{x},t)\cdot\nabla - \mathbf{b} = \mathbf{0} \tag{1}$$

with boundary and initial conditions given as follows:

$$\begin{aligned} &\boldsymbol{\sigma}(\mathbf{x},t)\cdot\mathbf{n} = \mathbf{h} && \mathbf{x}\in\Gamma_h \\ &\mathbf{u}(\mathbf{x},t) = \mathbf{g} && \mathbf{x}\in\Gamma_g \\ &\dot{\mathbf{u}}(\mathbf{x},0) = \mathbf{v}_0 && \mathbf{x}\in\Gamma_t \end{aligned} \tag{2}$$

where ρ is the material density, $\boldsymbol{\sigma}(\mathbf{x},t)$ is the Cauchy stress, $\mathbf{h}$ is the surface traction applied on the Neumann boundary Γ_h and $\mathbf{n}$ is the outward normal, $\mathbf{b}$ is the body force, $\mathbf{g}$ is the essential boundary condition applied on the Dirichlet boundary Γ_g, and v_0 is the initial velocity applied on the boundary Γ_t, which could be the whole problem domain.

The variational form can be written as:

$$\int_{\Omega_x}\rho\delta\Delta\mathbf{u}\bullet\ddot{\mathbf{u}}d\Omega = \int_{\Omega_x}\delta\Delta\mathbf{u}\bullet\mathbf{b}d\Omega + \int_{\Gamma_h}\delta\Delta\mathbf{u}\bullet\mathbf{h}d\Gamma - \int_{\Omega_x}\delta\Delta\boldsymbol{\varepsilon}:\boldsymbol{\sigma}d\Omega \tag{3}$$

Correspondingly, the semi-discrete equation based on meshfree approximation can be derived as:

$$\mathbf{M}\ddot{\mathbf{u}} = \mathbf{f}^{ext} - \mathbf{f}^{\text{int}} \tag{4}$$

where

$$\mathbf{f}_I^{ext} = \int_{\Gamma_h} \Phi_I \mathbf{h} d\Gamma + \int_{\Omega_x} \Phi_I \mathbf{b} d\Omega \tag{5}$$

$$\mathbf{f}_I^{\text{int}} = \int_{\Omega_I} \mathbf{B}_I^T \boldsymbol{\Sigma} d\Omega \tag{6}$$

where Φ_I is the meshfree shape function of displacement approximation, $\mathbf{B}_I$ is the gradient of shape function, and $\boldsymbol{\Sigma}$ is the stress vector determined by material constitutive law and is defined as:

$$\boldsymbol{\Sigma} = \left[\sigma_{11} \;\; \sigma_{22} \;\; \sigma_{33} \;\; \sigma_{12} \;\; \sigma_{23} \;\; \sigma_{31}\right]^T \tag{7}$$

The general form of meshfree displacement approximation can be written as:

$$\mathbf{u}^h(\mathbf{x},t) = \sum_{K=1}^{NP} \Psi_K(\mathbf{x}) \mathbf{d}_K(t) \tag{8}$$

where $\Psi_K(\mathbf{x})$ is the regular meshfree shape function.

To integrate Eq.(6) efficiently, direct nodal integration (DNI) is used in this study. However, DNI is known to suffer from rank deficiency [7]. To remove this instability, a penalty based strain gradient stabilization is derived from displacement smoothing theory [1, 2, 3] and thus the numerical method is named as the smoothed particle Galerkin (SPG). The displacement smoothing is given as:

$$\bar{\mathbf{u}}^h(\mathbf{x},t) = \sum_{K=1}^{NP} w_K(\mathbf{x}) \mathbf{u}^h(\mathbf{x}_K,t) \equiv \sum_{K=1}^{NP} \Phi_K(\mathbf{x}) \mathbf{d}_K(t) \tag{9}$$

$$\Phi_K(\mathbf{x}) = \sum_{I=1}^{NP} w_I(\mathbf{x}) \Psi_K(\mathbf{x}_I) \tag{10}$$

where $\Phi_K(\mathbf{x})$ is the SPG shape function, and $w_K(\mathbf{x})$ is the displacement smoothing function, which could be, in general, different from the displacement approximation shape function. However, for simplicity and efficiency, it is usually taken as the same shape function, and consequently, the SPG shape function and its derivatives can be written as:

$$\Phi_K(\mathbf{x}) = \sum_{I=1}^{NP} \Psi_I(\mathbf{x}) \Psi_K(\mathbf{x}_I) \tag{11}$$

$$\Phi_{K,i}(\mathbf{x}) = \sum_{I=1}^{NP} \Psi_{I,i}(\mathbf{x}) \Psi_K(\mathbf{x}_I) \tag{12}$$

Finally, the gradient of the SPG shape function can be derived as:

$$\mathbf{B}_K(\mathbf{x}) = \begin{bmatrix} \Phi_{K,x}(\mathbf{x}) & 0 & 0 \\ 0 & \Phi_{K,y}(\mathbf{x}) & 0 \\ 0 & 0 & \Phi_{K,z}(\mathbf{x}) \\ \Phi_{K,y}(\mathbf{x}) & \Phi_{K,x}(\mathbf{x}) & 0 \\ 0 & \Phi_{K,z}(\mathbf{x}) & \Phi_{K,y}(\mathbf{x}) \\ \Phi_{K,z}(\mathbf{x}) & 0 & \Phi_{K,x}(\mathbf{x}) \end{bmatrix} \tag{13}$$

The derivation of the stabilization term and numerical algorithms for implementation are documented elsewhere [2, 5, 6] and thus they are omitted in this paper. The critical time step for the central difference time integration of Eq.(4) in the explicit dynamics analysis is governed by the Courant-Friedrichs-Lewy (CFL) condition and is determined following the developments in [8] for the numerical studies. It is worthwhile to note that

the meshfree time steps in the explicit dynamics analysis are controlled implicitly [8] by the radius size of the support of the SPG shape function in the displacement approximation instead of the closet nodal distance or element size as in the FEM; therefore they will not be cut down abruptly due to severe material deformation.

2.2. Strain-based bond failure mechanism

Destructive manufacturing processes, such as metal blanking, cutting, drilling, grinding, and riveting are very large deformation processes with material failure and separation. If these processes are analyzed by continuum mechanics, excessive straining will inevitably occur due to the severe deformation. As a result, the discontinuity in the displacement field is not captured which leads to spurious damage growth in material failure analysis. The spurious damage growth eventually causes the numerical breakdown due to non-unique mapping between the current and the reference configuration in a Lagrangian analysis.

A strain-based bond failure mechanism is implemented in the SPG framework so that displacement discontinuity can be captured and furthermore, the spurious damage growth is prevented. It's named "strain-based" because the failure criterion is the effective plastic strain calculated from the material constitutive law in the application to manufacturing process analysis. In specific, two neighboring particles are considered disconnected during the meshfree neighbor particle searching whenever their averaged effective plastic strain and relative stretch reach their respective critical values. In other words, for a pair of nodes *K* and *J*, the SPG shape function in Eq.(11) can be redefined as:

$$\Phi_K\left(\mathbf{x}_J\right)=\begin{cases}0 & \text{if } \bar{\varepsilon}^p_{KJ}>\bar{\varepsilon}^p_{crit} \text{ and } e_{KJ}>e_{crit}\\ \sum_{I=1}^{NP}\Psi_I\left(\mathbf{x}_J\right)\Psi_K\left(\mathbf{x}_I\right) & \text{Otherwise}\end{cases} \tag{14}$$

where $\bar{\varepsilon}^p_{KJ}=\left[\bar{\varepsilon}^p\left(\mathbf{x}_K\right)+\bar{\varepsilon}^p\left(\mathbf{x}_J\right)\right]/2$ is the averaged effective plastic strain at nodes K and J and $\bar{\varepsilon}^p_{crit}$ is its critical value; $e_{KJ}=\left\|\mathbf{x}_K-\mathbf{x}_J\right\|/\left\|\mathbf{X}_K-\mathbf{X}_J\right\|$ is the relative stretch between nodes K and J, where $\mathbf{x}$ and $\mathbf{X}$ are the current and reference coordinates.

The bond failure mechanism is illustrated in Figure 1. The big blue circle represents the support of node 2, and the big red circle represents the support of node 1. Initially, there are 5 bonds connected to node 2, i.e., bonds 2-1, 2-8, 2-9, 2-3, and 2-10. There are 7 bonds connected to node 1, i.e., bonds 1-2, 1-8, 1-7, 1-5, 1-4, 1-6, and 1-10. Assume the failure criteria for bond 1-2 are satisfied, i.e., $\bar{\varepsilon}^p_{12}=\left[\bar{\varepsilon}^p\left(\mathbf{x}_1\right)+\bar{\varepsilon}^p\left(\mathbf{x}_2\right)\right]/2>\bar{\varepsilon}^p_{crit}$ and $e_{12}>e_{crit}$, then bond 1-2 is broken. Therefore, $\Phi_2\left(\mathbf{x}_1\right)=0$ and $\Phi_1\left(\mathbf{x}_2\right)=0$. However, $\Phi_2\left(\mathbf{x}_k\right)\neq 0\ \ k=3,8,9,10$ and $\Phi_1\left(\mathbf{x}_k\right)\neq 0\ \ k=4,5,6,7,8,10$, which means all the other bonds except bond 1-2 are still connecting. This indicates that the state variables (i.e., stress and strain) at nodes 1 and 2 will still evolve regularly according to the deformation and material law. The only change is that their neighboring particles have one less node. Therefore, unlike the finite element failure mechanism, where the element is eroded (loss of mass) according to an ad-hoc criterion and the element stress is set to zero (loss of momentum) when failure occurs, the SPG bond failure mechanism preserves the mass and momentum. It should be pointed out that since the effective plastic strain at each

particle is monotonically increasing during the course of deformation, the kinematic disconnection (i.e., bond failure) between two particles in a pair is considered as a permanent and irreversible process. This is a substantial characteristic of the SPG method in metal ductile failure analysis since the non-physical material self – healing issue is completely exempted from the modeling of the failure process.

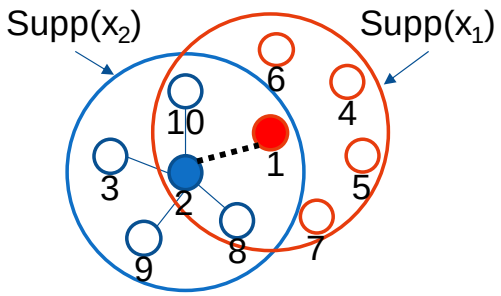

Figure 1. Illustration of SPG bond failure mechanism.

2.3. LS-DYNA keywords for SPG analysis

The SPG formulation has been implemented into the commercial software LS-DYNA® [9]. Most of the SPG functions are available in R10, which was released on July 5, 2017. To setup an SPG analysis, the exact same discretization as for an FEM analysis is used except an additional flag to activate the SPG formulation for the particular part in the model that is to be approximated by SPG.

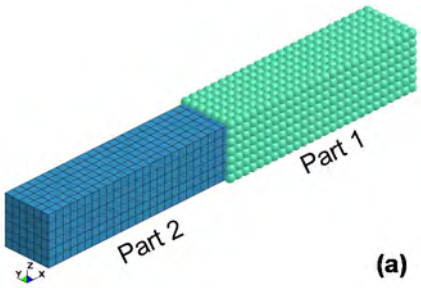


```
*PART
         1       1       4       1       0       0       0       1
*PART
         2       2       4       1       5       0       0       1
*SECTION_SOLID_SPG
         1      47
$#      DX      DY      DZ  ISPLINE  KERNEL  LSCALE  SMSTEP  SWTIME
       1.6     1.6     1.6                1                      15
$    IDAM      FS  STRETCH     ITB
         1    0.45    1.20       1
*SECTION_SOLID
$     secid   elform
         2       1
```

(b)

Figure 2. Setup for SPG analysis: (a) discretization of problem domain, (b) control cards.

Figure 2 illustrates the setup for an SPG analysis. The problem domain is all discretized by finite elements initially and then it's separated into part 1 and part 2. Part 1 is flagged to SPG formulation through SECID = 1 which is defined by

*SECTION_SOLID_SPG, and is displayed as spheres since it's a particle method. Part 2 is assigned to regular FEM formulation through SECID = 2. However, *ELEMENT_SOLID is used for both parts (i.e., no special keyword for the "element" output for SPG discretization). The interface between part 1 and part 2 shares common nodes. The coupling between FEM and SPG is naturally dealt with by the shared nodes [6]. On the *SECTION_SOLID_SPG card, DX, DY, and DZ are the normalized support size in x-, y- and z-direction respectively; KERNEL indicates the type of the meshfree kernel function (0-update Lagrangian, 1-Eulerian, 2-pseudo Lagrangian); SMSTEP gives the number of time steps for kernel updating; FS defines the critical effective plastic strain $\bar{\varepsilon}^p_{crit}$ for the SPG bond failure; and "STRETCH" is the critical relative stretch e_{crit} which should always be no less 1.0 such that SPG bond only fails under relative tension.

3. Application of the SPG method

To demonstrate the effectiveness of the SPG method in modeling ductile failure in destructive manufacturing processes, a metal friction drilling process is analyzed and compared with limited experimental data in this section. If not otherwise specified, the normalized SPG support size is 1.6 and the Eulerian kernel is updated every 15 time steps in the explicit dynamic analysis.

3.1. Drilling of AISI 304 steel

A disk of AISI 304 stainless steel with 18 mm diameter and 1.5 mm thickness was used in the experiment of a friction drilling process [10]. The geometry of the tool is shown in Figure 3 (a). The setup and the numerical discretization of the drilling process are shown in Figure 3 (b). The tool is modeled by rigid tetrahedral finite elements. The tool rotates at 3000 rpm and plunges at 100 mm/min in the test. The central area of 6.4 mm by 6.4 mm is discretized by SPG particles with nodal distance approximately at 0.2 mm. The remaining workpiece is modeled by hexagonal finite elements. The perimeter of the workpiece is clamped. The Johnson – Cook material law is applied for the workpiece for both the SPG and finite element discretizations. However, the Johnson – Cook damage law is not used since the failure process is modeled by the SPG bond failure mechanism. According to efunda (www.efunda.com), the Young's modulus of the workpiece is set to 193 GPa, and the yield strength is set to 205 MPa, and the effective plastic strain for bond failure is set to 0.4. The other material parameters are taken from the reference [10]. The coefficient of friction (COF) between the tool and the workpiece is set to 0.2 for the node-to-surface contact in the numerical analysis.

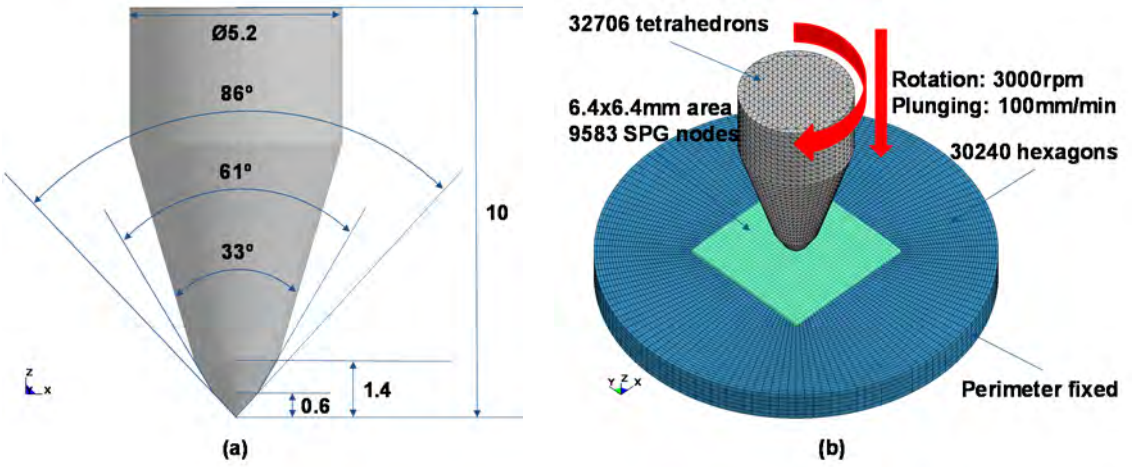

Figure 3. Friction drilling: (a) tool geometry, (b) discretization and boundary conditions.

Figure 4 shows the thrust force and torque histories obtained from the coupled FEM/SPG and FEM simulations respectively. The thicker lines are the test data and the lighter curves are the numerical results. Considering that in the test, the temperature on the upper side of the plate at the contact zone reaches 569ºC, but the thermal effect is ignored in the simulation, the coupled FEM/SPG solution matches the test data reasonably well. On the other hand, due to loss of mass and momentum in FEM with erosion process, the FEM approach does not build up force and momentum. Figure 5 shows the evolution of effective plastic strain in the drilling process. Material fracture on the back side is clearly observed. It is important to point out that the effective plastic strain for SPG bond failure is 0.4, but the effective plastic strain in the material reaches 0.7 or more. The reason is some material continues to evolve stress and strain in compression state even after bond failure (see the explanation in Section 2.2) until all the bonds fail.

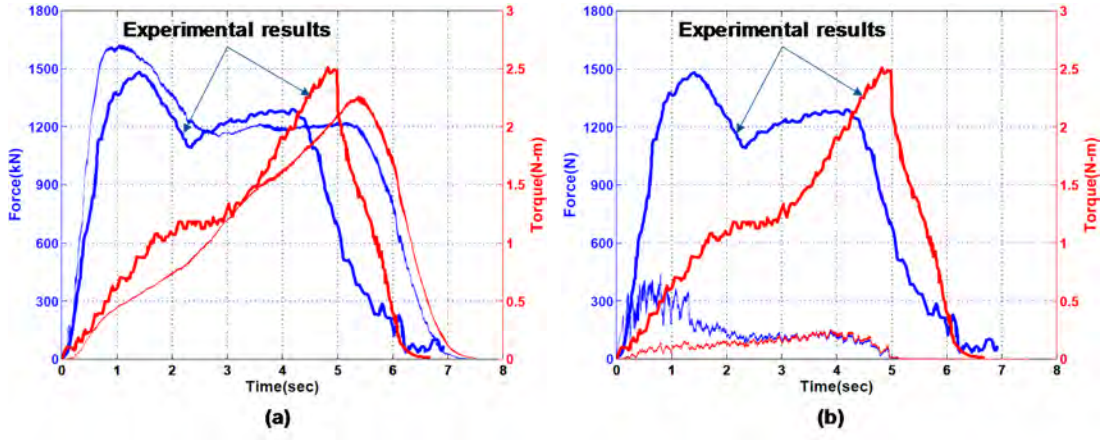

Figure 4. Drilling - thrust force and torque histories: (a) SPG solution, (b) FEM solution.

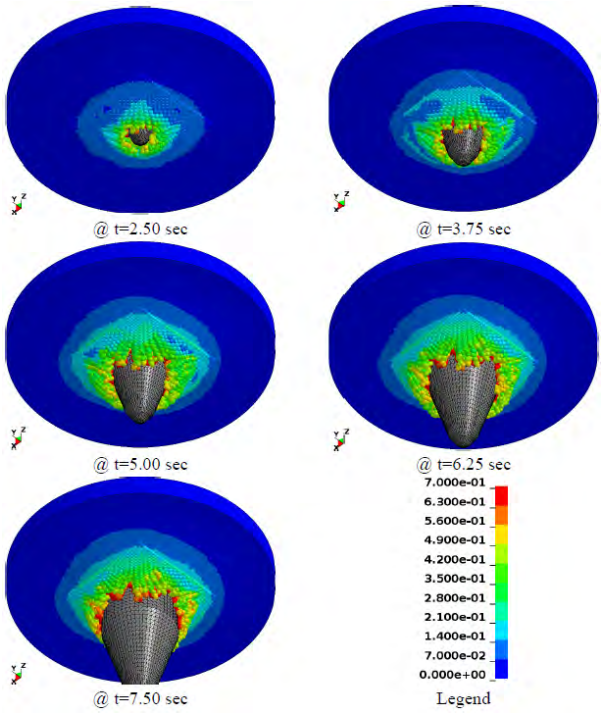

Figure 5. Drilling: progressive deformation (SPG solution).

3.2. Parameter study

3.2.1. Sensitivity to bond failure criteria

Figure 6 shows the thrust force and torque histories for two sets of bond failure criteria, i.e., the effective plastic strain of 0.4 and 0.7 for SPG bond failure respectively. It seems the SPG bond failure criteria do not have any impact on the numerical results. It should be pointed out that the COF used for these analyses is 0.3, which leads to a much higher torque than the test measurements, and the Young's modulus and yield strength for the workpiece is 207.8 GPa and 280 MPa respectively, which leads to a quite high thrust force compared with the test measurements.

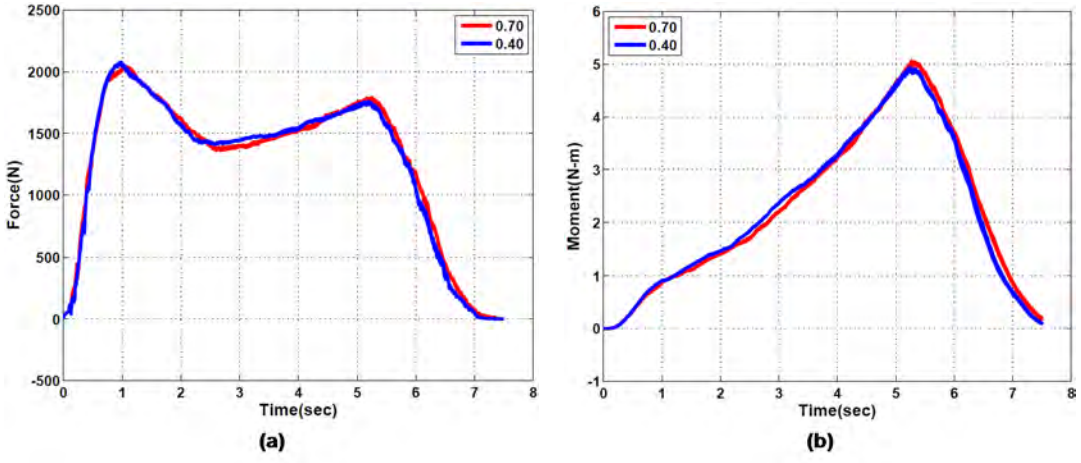

Figure 6. Drilling – sensitivity to SPG bond failure criteria: (a) thrust force, (b) torque.

3.2.2. Sensitivity to coefficient of friction (COF) and material strength

Figure 7 shows the thrust force and torque histories for two materials and two COFs. "0.15" and "0.20" on the legend refer to COF of 0.15 and 0.20 respectively. "m1" refers to a material with Young's modulus of 207.8 GPa and yield strength of 280 MPa, and "m2" refers to a material with Young's modulus of 193 GPa and yield strength of 205 MPa. Figure 7 (a) indicates that the thrust force has a high dependence on material strength while very limited dependence on COF. Figure 7 (b) reveals that the torque highly depends on the interface friction, which is physical since the torque is generated solely due to friction. These observations imply that it is crucial to physically model the material and the interface to obtain reliable numerical results.

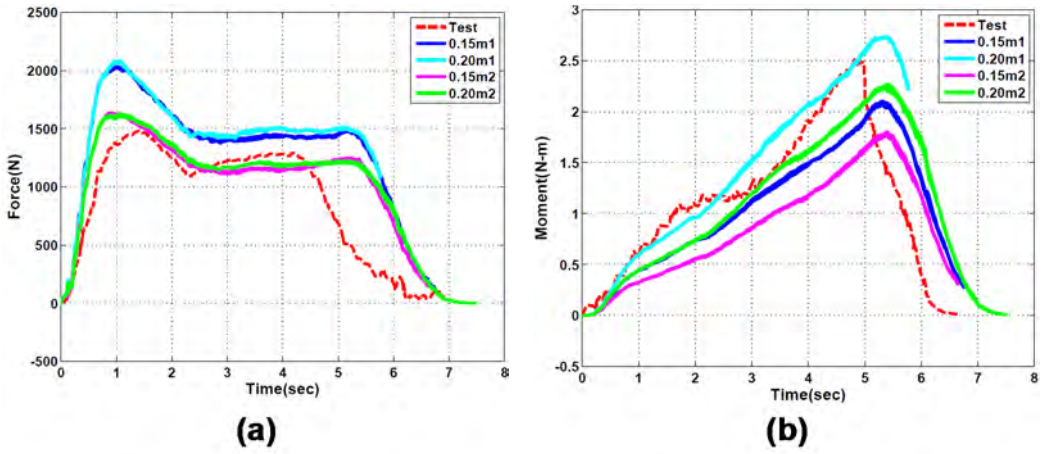

Figure 7. Drilling – sensitivity to COF and yield strength: (a) thrust force, (b) torque.

3.2.3. Sensitivity to kernel update frequency

Figure 8 shows the thrust force and torque histories for various SPG kernel update frequencies. The SPG kernels are updated every 5, 15 and 30 explicit time steps in the calculations respectively. It is observed that both the thrust force and the torque do not show too much dependence on the kernel update frequency.

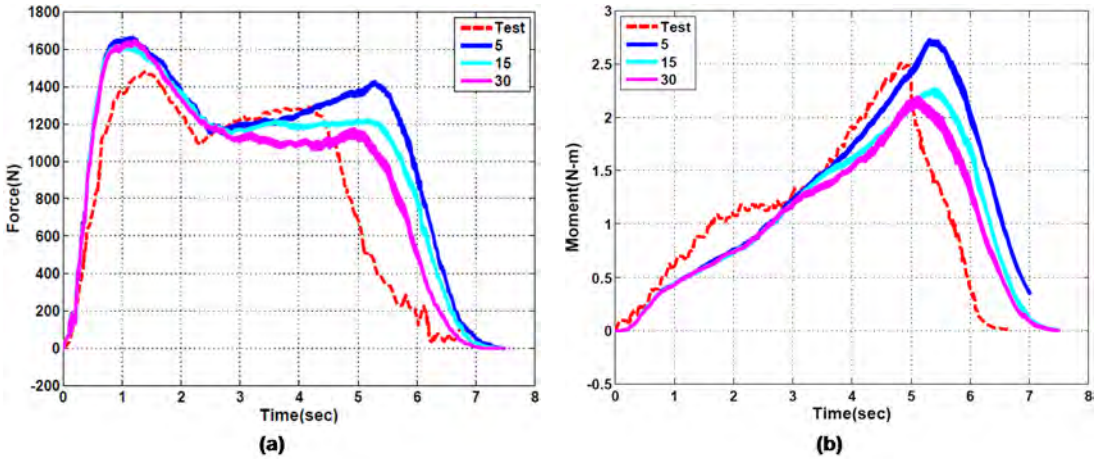

Figure 8. Drilling – sensitivity to kernel update frequency: (a) thrust force, (b) torque.

3.2.4. Sensitivity to normalized support size

Figure 9 shows the thrust force and torque histories for various normalized support sizes. The normalized support sizes used in the calculations are 1.6 and 1.8 respectively. Not very much sensitivity is observed if the normalized support size is in the range of recommendation for analysis manufacturing processes, which is 1.6 ~ 1.8.

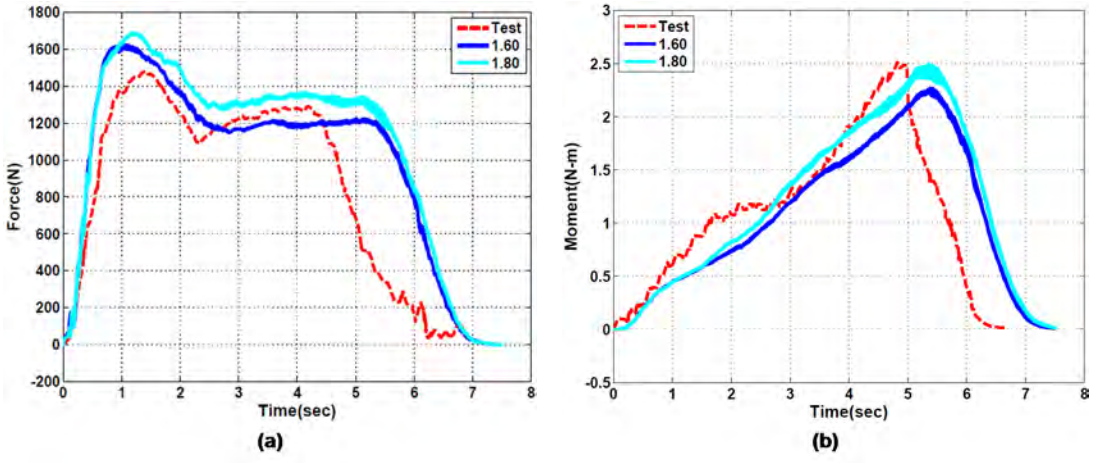

Figure 9. Drilling – sensitivity to normalized support size: (a) thrust force, (b) torque.

4. Conclusion

In this paper, the smoothed particle Galerkin (SPG) method is applied in the analysis of ductile failure in destructive manufacturing processes. The SPG weak form is efficiently integrated by the direct nodal integration (DNI) scheme, while the rank deficiency of DNI is alleviated by a non-residual penalty type stabilization derived from displacement smoothing theory. Meanwhile, to deal with material failure in destructive manufacturing processes, a strain-based bond failure mechanism is implemented. With the bond failure mechanism, no element or mass is deleted after material failure, and thus mass and momentum are conserved, which is very important in correctly predicting reaction forces and is in sharp comparison with element erosion type of failure mechanism in finite element models.

A friction drilling process is analyzed with the SPG method. Very promising results are obtained both qualitatively and quantitatively. The numerical results show sensitivity to material strength, coefficient of friction between the tool and workpiece, which is physical. On the other hand, the results do not show too much sensitivity to the bond failure criteria, which makes the numerical scheme robust and reliable since the major criteria for bond failure do not need to be tuned, which compares dramatically different from element erosion type finite element analysis. The numerical results do not show significant dependence on other SPG parameters such as the SPG support size and kernel update frequency either.

Acknowledgements

The authors wish to thank Dr. John O. Hallquist of LSTC for his support to this research.

Reference:

1. Wu CT, Koishi M, Hu W. A displacement smoothing induced strain gradient stabilization for the meshfree Galerkin nodal integration method. Comput. Mech. 2015;56:19-37.
2. Wu CT, Chi SW, Koishi M, Wu Y. Strain gradient stabilization with dual stress points for the meshfree nodal integration method in inelastic analysis. Int. J. Numer. Methods Engrg. 2016;107:3-30.
3. Wu CT, Wu Y, Koishi M. A strain-morphed nonlocal meshfree method for the regularized particle simulation of elastic-damage induced strain localization problems. Comput. Mech. 2015;56:1039-1054.
4. Wu CT, Ma N, Takada K, Okada H. A meshfree continuous-discontinuous approach for the ductile fracture modeling in explicit dynamics analysis. Comput. Mech. 2016;58:391-409.
5. Wu CT, Wu Y, Crawford JE, Magallanes JM. Three dimensional concrete impact and penetration simulations using the smoothed particle Galerkin method. Int. J. Impact Engrg. 2017;106:1-17.
6. Wu CT, Bui TQ, Wu Y, Luo TL, Wang M, Liao CC, Chen PY, Lai YS. Numerical and experimental validation of a particle Galerkin method for metal grinding simulation. Comput. Mech. 2017, accepted for publication and pre-view version is available on-line.
7. Chen JS, Wu CT, Yoon S, You Y. A stabilized conforming nodal integration for Galerkin Meshfree methods, Int. J. Numer. Methods Engrg. 2001:50:435-466.
8. Park CK, Wu CT, Kan CD. On the analysis of dispersion property and stable time step in meshfree method using the generalized meshfree approximation. Finite Elem. Anal. Des. 2011;47:683-697.
9. Hallquist JO. LS-DYNA® Keyword User's Manual, Livermore Software Technology Corporation, Livermore, California, 2006
10. Krasauskas P, Kilikevičius S, Česnavičius R, Pačenga D. Experimental analysis and numerical simulation of the stainless AISI 304 steel friction drilling process. Mechanika 2014;20(6):590-595